

Numerical simulations of tail formation in wind interactions with injected material

S. A. E. G. Falle,¹★ R. F. Coker,² J. M. Pittard,² J. E. Dyson² and T. W. Hartquist²

¹*Department of Applied Mathematics, University of Leeds, Leeds LS2 9JT*

²*Department of Physics and Astronomy, University of Leeds, Leeds LS2 9JT*

Accepted 2001 October 3. Received 2001 October 2; in original form 2001 August 23

ABSTRACT

A numerical simulation of the interaction of a hypersonic wind with a mass source shows that, downstream of the source, the injected material occupies a cone with a sizable opening angle. In contrast, the injected material is confined to a long, thin tail when the wind is transonic.

Key words: hydrodynamics – ISM: jets and outflows – ISM: structure.

1 INTRODUCTION

Inhomogeneities within a variety of diffuse sources including planetary nebulae (e.g. Meaburn et al. 1992; O’Dell, Henney & Burkert 2000), the environment around the Orion Nebula (e.g. Bally et al. 1998), and the interstellar medium of the Galactic Centre (Yusef-Zadeh & Morris 1991) possess long, thin ‘cometary’ tails. The idea that these are owing to shadowing of ionizing radiation has been thoroughly explored (e.g. Bertoldi 1989; Bertoldi & McKee 1990; Lefloch & Lazareff 1994; Henney et al. 1996, 1997; Cantó et al. 1998; Johnstone, Hollenbach & Bally 1998; Mellema et al. 1998; Richling & Yorke 1998; Stoerzer & Hollenbach 1999; Pavlakis et al. 2001).

Dyson, Hartquist & Biro (1993) suggested that, whereas the interaction of a highly supersonic wind with material evaporating at the local sound speed from a clump produces a broad tail, a subsonic or sonic wind leads to a long thin tail. In this paper, we use hydrodynamic calculations to explore this conjecture. An example of a situation for which this is relevant is provided by any of the many Helix Nebula globules having cometary tails. Dyson et al. (1989) argued that such globules must be cold and molecular, which means that the ionized material that is observed around such a globule contains only a small fraction of the mass of the globule. The time required to evaporate all of the molecular material in a globule is therefore much longer than any of the other relevant time-scales in the problem and the rate of evaporation may therefore be assumed to be constant. This will also be true of a dense cloud from which material is being ablated by a tenuous wind.

In Section 2 we describe the problem and derive some simple expressions in order to determine the appropriate parameters. The numerical results for both a hypersonic and transonic wind are discussed in Section 3 and Section 4 contains our conclusions.

2 THE MODEL

Since we are interested only in the qualitative features of the large-scale flow owing to the interaction of a wind with injected material, the actual details of the mass injection are unimportant and we merely have to ensure that the mass flux and velocity at the surface of the cloud have the appropriate values. This could be carried out by injecting mass in a thin region near the surface of the cloud, but it is more convenient to assume a uniform rate of mass injection within a sphere and then to use the analysis employed by Chevalier & Clegg (1985) and Cantó, Raga & Rodriguez (2000) to determine the appropriate parameters.

As we shall see, this procedure is simple and effective, but it does have the disadvantage that it can only model an isotropic flow from the surface of the cloud. However, although the mass loss is certainly not isotropic if it is driven by hydrodynamic ablation or radiative evaporation, the effect of such asymmetry is likely to be small at large distances from the cloud.

2.1 The mass-injection region

Suppose that we have a steady spherically symmetric isothermal flow with a mass-injection rate, $Q(r)$, per unit volume. If the wind does not affect the flow inside the cloud, then the relevant equations are

$$\frac{1}{r^2} \frac{d}{dr} r^2 \rho v = Q(r) \quad \text{continuity,} \quad (1)$$

$$v \frac{dv}{dr} = -\frac{a^2}{\rho} \frac{d\rho}{dr} - \frac{Qv}{\rho} \quad \text{momentum.} \quad (2)$$

Using (1) in (2) gives

$$(v^2 - a^2) \frac{dv}{dr} = a^2 \left(\frac{2v}{r} - \frac{Q}{\rho} \right) - \frac{Qv^2}{\rho}. \quad (3)$$

If the external pressure is sufficiently low, then the flow must become supersonic at some point r_s (see e.g. Chevalier & Clegg

★E-mail: sam@amsta.leeds.ac.uk

1985). Equation (3) tells us that the solution can only pass smoothly through the sonic point if

$$r_s = \frac{\rho a}{Q}.$$

The position of the sonic point is determined by equating the rate of mass-injection interior to the sonic point to the mass flux at the sonic point. This gives

$$\int_0^{r_s} r^2 Q(r) dr = r_s^3 Q(r_s), \quad (4)$$

and the density at the sonic point is then given by

$$\rho_s = \frac{1}{r_s^2 a} \int_0^{r_s} r^2 Q(r) dr.$$

Equation (4) does not have a solution for arbitrary $Q(r)$, in particular there is no solution if $Q(r) = \text{constant}$ everywhere. However, if $Q(r) = Q = \text{constant}$ inside some radius r_g and then decreases rapidly to zero in some small region $r_g \leq r \leq r_g + \epsilon$, then the integral in (4) is approximately equal to $Q r_g^3/3$ and it is clear that the sonic point must lie somewhere in $r_g \leq r \leq r_g + \epsilon$. If we now let $\epsilon \rightarrow 0$, we get a uniform injection rate inside $r = r_g$, the flow becomes sonic at $r = r_g$ and the density at the sonic point is

$$\rho_s = \frac{r_g Q}{3a}.$$

Since we do not want the wind to affect the flow in the injection region, we have to ensure that the ram pressure of the injected material at r_g is larger than that in the wind, i.e. we require

$$a^2 \rho_s = \frac{a r_g Q}{3} \geq \rho_w v_w^2, \quad (5)$$

where ρ_w , v_w are the wind density and velocity.

2.2 Computational details

In order to ensure that the injected gas remains isothermal and the wind gas behaves adiabatically, we use a passive scalar, α , which is unity in the globule gas and zero in the wind gas. The source term in the energy equation is then

$$K \alpha \rho (1 - T), \quad (6)$$

where K is large enough to ensure that the temperature always remains close to unity in the globule gas. Inside the globule we added an extra energy source

$$\frac{Q}{(\gamma - 1)}$$

so that the gas is injected with temperature unity.

For the supersonic case we can simply use the Euler equations, but this is not satisfactory for the transonic case since the wind flow separates and produces a turbulent wake downstream of the injection region. No calculation based on the axisymmetric Euler equations can hope to capture this, so the only viable option is to use a turbulence model. There are many possibilities, but since we are only interested in the qualitative features of the flow, a simple $k - \epsilon$ model should suffice. Although there exist much more sophisticated models, experience suggests that it is not too bad for flows of this type (see e.g. Cumber et al. 1994). The details can be found in Falle (1994).

All the calculations were carried out in axisymmetry using the hierarchical adaptive grid code, Cobra (Falle & Giddings 1993).

Cobra uses a hierarchy of grids $G^0 \dots G^N$ such that the mesh spacing on grid G^n is $\Delta x_0/2^n$. Grids G^0 and G^1 cover the whole domain, but the finer grids only exist where they are needed. The solution at each position is calculated on all grids that exist there and the difference between these solutions is used to control refinement. In order to ensure Courant number matching at the boundaries between coarse and fine grids, the time-step on grid G^n is $\Delta t_0/2^n$ where Δt_0 is the time-step on G^0 .

Such a hierarchical grid structure not only improves the efficiency by confining the fine grids to where they are needed, but it also makes it possible to use a full approximation multigrid algorithm to accelerate the convergence to the steady state (see e.g. Brandt 1977).

3 RESULTS

3.1 Hypersonic wind

We choose units such that $r_g = 1$, $a = 1$, $\rho_w = 1$ and then set $v_w = 20$. Since the sound speed in the globule gas is about 10 km s^{-1} , this corresponds to a wind speed of 200 km s^{-1} , which is appropriate for a young stellar object. However, the actual wind speed does not matter as long as the external Mach number is large. Equation (5) then tells us that we need $Q \geq 1200$, in order to prevent the wind from penetrating the mass-injection region. However, in the supersonic case, a better estimate is obtained by replacing $\rho_w v_w^2$ by the pressure behind a stationary normal shock in the wind. This gives

$$Q \geq \frac{6}{(\gamma + 1)} \frac{\rho_w v_w^2}{a r_g} = 900$$

for $\gamma = 5/3$. We set $Q = 1000$ in order to ensure that the interaction occurs slightly outside the mass-injection region. The coefficient, K , in (6) was set to 50, which is large enough to ensure that the temperature in the globule gas is always within 5 per cent of the equilibrium temperature except in the immediate vicinity of the shocks in the tail.

The computational domain is $0 \leq r \leq 12.5$, $-20 \leq z \leq 5$ with the mass-injection region centred at the origin. 5 grid levels $G^0 \dots G^4$, were used with G^0 being 25×50 and G^4 400×800 . The fact that there is very little difference between the solutions on G^3 and G^4 shows that this resolution is more than adequate.

Fig. 1 shows the density, pressure and z -velocity, together with the regions occupied by the finest grid. The wind is decelerated by a bow shock and is separated from the injected material by a contact discontinuity. The injected gas behaves like an under-expanded jet and contains a shock cell downstream of the injection region. However, the important point is that the injected material is not confined to a long thin tail, instead the contact discontinuity has a radius of 8 at $z = -20$. Although its radius does not appear to be increasing significantly at this point, it is already much larger than the size of the injection region. As we shall see, this is in stark contrast to what happens in the sonic case.

3.2 Sonic wind

The particular globule that we are considering is only one of many that the wind encounters, which means that the total rate of mass injection will eventually become comparable to the mass flux in the wind. In that case one expects that the Mach number of the wind will tend towards unity (e.g. Hartquist et al. 1986), and it is

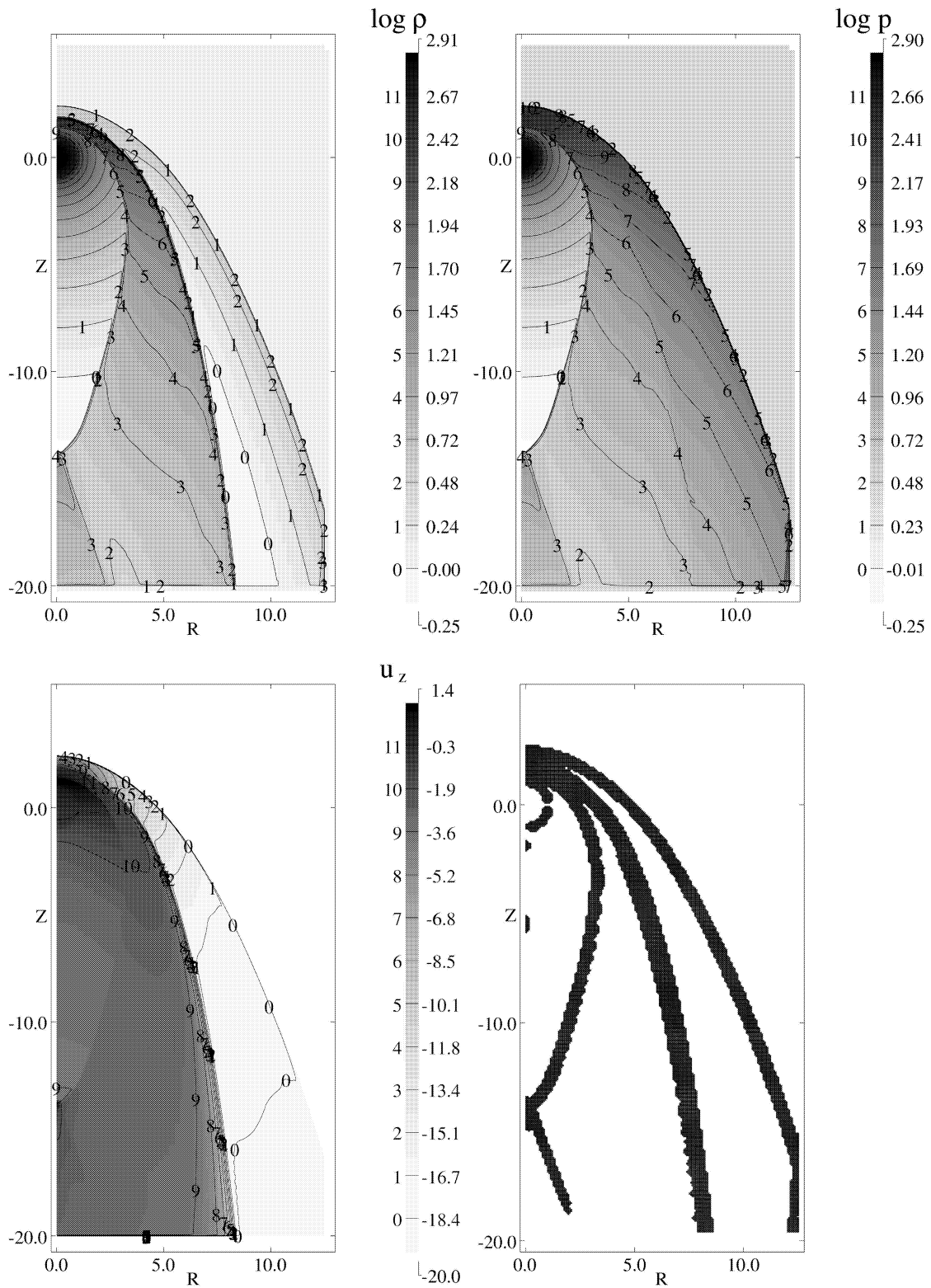


Figure 1. Density, pressure, z -velocity and G^4 for the supersonic case.

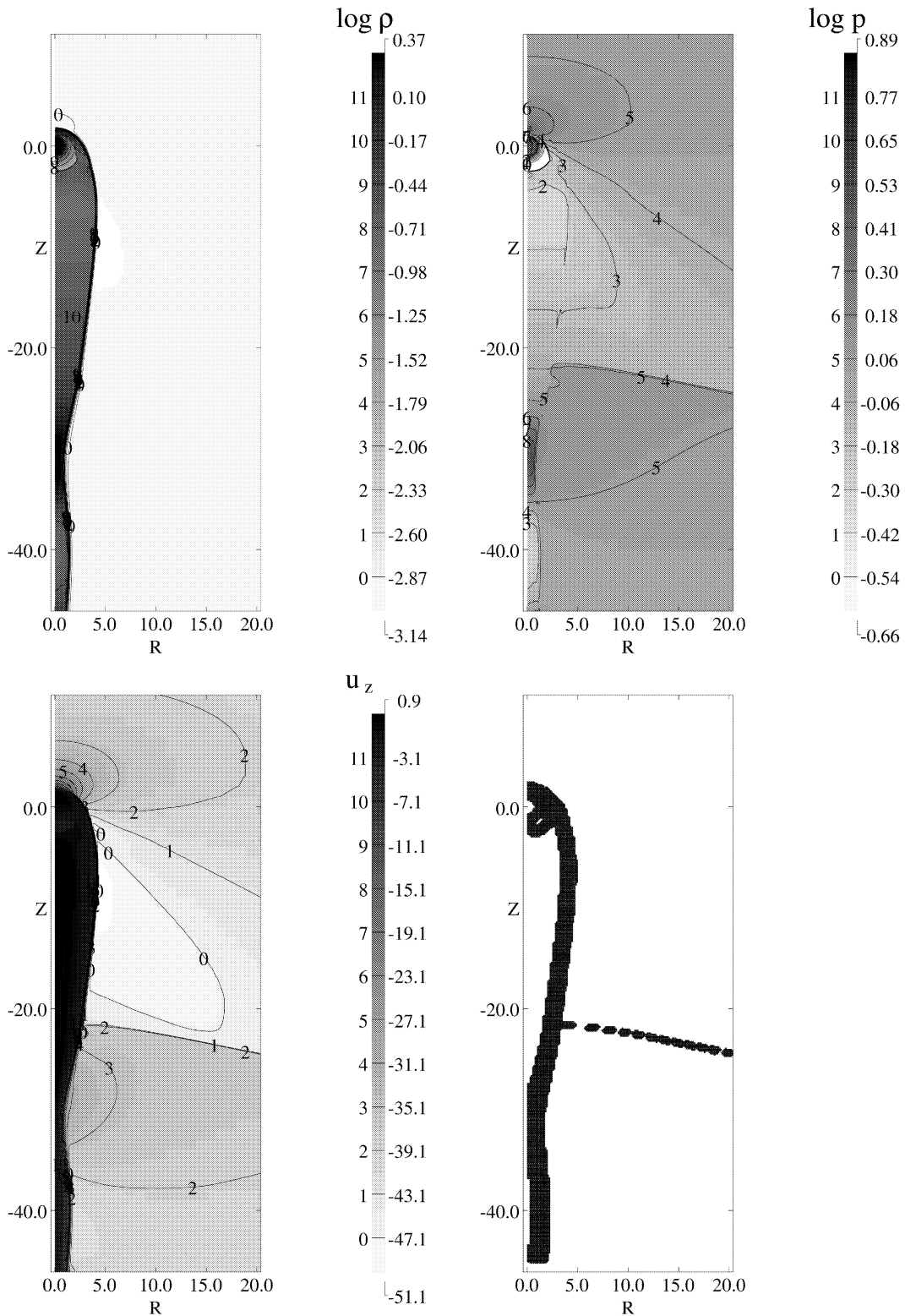


Figure 2. Density, pressure, z -velocity and G^5 for the sonic case.

therefore reasonable to look at the interaction of the mass-injection region with a sonic wind.

In this case we set $r_g = 1$, $a = 1$ as before but now $\rho_w = 10^{-3}$, $v_w = 40.825$, giving a Mach number of unity in the undisturbed wind. The condition (5) gives $Q \geq 5$, which is a quite a good estimate for this case since there is no shock upstream of the injection region. We therefore set $Q = 5$. The coefficient, K , in (6) is 10^2 , which, as in the previous case, is large enough to keep the temperature in the injected gas within 5 per cent of its equilibrium value. In order to ensure that the boundaries had no effect on the solution, the computational domain has to be very large, $0 \leq r \leq 50$, $-50 \leq z \leq 30$. This would have made the calculation extremely expensive were it not for the fact that the fine grids are only required near the axis.

It can be seen from Fig. 2 that the flow is very different from the supersonic case. There is no bow shock, but there is a weak tail shock in the wind downstream of the object. The injected material remains in rough pressure equilibrium with the wind, it contains no shock cells and eventually becomes confined to a region whose radius is of about the same order as the size of the injection region.

4 CONCLUSIONS

The results described in Section 3 indicate that, once the flow becomes steady, a long, thin tail forms downstream of a source that is injecting mass at close to the sound speed into a transonic, tenuous wind. As mentioned in the introduction, essentially steady injection is possible from a source that is much colder and denser than its surroundings. The clumps in Orion and in planetary nebulae that are observed to have tails do indeed have this property.

Whilst the shadowing of ionizing radiation must have an effect on these tails, this does not, by itself, provide an obvious explanation for the existence of both broad and narrow tails in the planetary nebula Abell 30 (Borkowski, Harrington & Tsvetanov 1995). Our calculations lend support to the suggestion by Hartquist & Dyson (1996) that the broad tails are in regions where the tenuous material is flowing supersonically and the narrow ones where it is subsonic or transonic. Such variations in the Mach number of the wind are to be expected, since a steady wind, in which the mass loading is significant out to some distance and then becomes negligible, would start supersonic, become subsonic at a shock and then pass smoothly through a sonic point (Arthur et al. 1994; Williams et al. 1995).

It therefore seems reasonable to conclude that long thin tails should occur naturally in regions in which the global flows are sufficiently mass loaded provided that the pressure of the injected material is not large compared to that of the surrounding tenuous material. Since there are indications that the mass loading

is substantial in the part of Orion where tails are observed (S. J. Arthur, private communication), our results may also be relevant to the Orion tails as well as those in planetary nebulae.

ACKNOWLEDGMENTS

We thank the referee, Alex Raga, for his constructive comments on the original version. RFC and JMP acknowledge support from PPARC during the course of this work.

REFERENCES

- Arthur S. J., Dyson J. E., Hartquist T. W., 1994, *MNRAS*, 269, 1117
 Bally J., Sutherland R. S., Devine D., Johnstone D., 1998, *AJ*, 116, 293
 Bertoldi F., 1989, *ApJ*, 346, 735
 Bertoldi F., McKee C. F., 1990, *ApJ*, 354, 529
 Borkowski K. J., Harrington J. P., Tsvetanov Z. I., 1995, *ApJ*, 449, L143
 Brandt A., 1977, *Math. Comput.*, 31, 333
 Cantó J., Raga A., Steffen W., Shapiro P., 1998, *ApJ*, 502, 695
 Cantó J., Raga A. C., Rodriguez L. F., 2000, *ApJ*, 536, 896
 Chevalier R. A., Clegg A. W., 1985, *Nat*, 317, 44
 Cumber P. S., Fairweather M., Falle S. A. E. G., Giddings J. R., 1994, *Trans. ASME J. Fluids Eng.*, 116, 707
 Dyson J. E., Hartquist T. W., Pettini M., Smith L. J., 1989, *MNRAS*, 241, 625
 Dyson J. E., Hartquist T. W., Biro S., 1993, *MNRAS*, 261, 430
 Falle S. A. E. G., 1994, *MNRAS*, 269, 607
 Falle S. A. E. G., Giddings J. R., 1993, in Morton K. W., Baines M. J., eds, *Numerical Methods for Fluid Dynamics 4*. Clarendon Press, Oxford, p. 335
 Hartquist T. W., Dyson J. E., 1996, *Ap&SS*, 245, 263
 Hartquist T. W., Dyson J. E., Pettini M., Smith L. J., 1986, *MNRAS*, 221, 715
 Henney W. J., Raga A. C., Lizano S., Curiel S., 1996, *ApJ*, 456, 216
 Henney W. J., Meaburn J., Raga A. C., Massey R., 1997, *A&A*, 324, 656
 Johnstone D., Hollenbach D., Bally J., 1998, *ApJ*, 499, 758
 Lefloch B., Lazereff B., 1994, *A&A*, 289, 559
 Meaburn J., Walsh J. R., Clegg R. E. S., Walton N. A., Taylor D., Berry D. S., 1992, *MNRAS*, 255, 177
 Mellema G., Raga A. C., Cantó J., Lundqvist P., Balick B., Steffen W., Noriega-Crespo A., 1998, *A&A*, 331, 335
 O'Dell C. R., Henney W. J., Burkert A., 2000, *AJ*, 119, 2910
 Pavlakis K. G., Williams R. J. R., Dyson J. E., Falle S. A. E. G., Hartquist T. W., 2001, *A&A*, 369, 263
 Richling S., Yorke H. W., 1998, *A&A*, 340, 508
 Stoerzer H., Hollenbach D., 1999, *ApJ*, 515, 669
 Yusef-Zadeh F., Morris M., 1991, *ApJ*, 371, L59
 Williams R. J. R., Hartquist T. W., Dyson J. E., 1995, *ApJ*, 446, 759

This paper has been typeset from a $\text{\TeX/L\AA}\text{\TeX}$ file prepared by the author.